Toxicity and action mechanisms of silver nanoparticles against the mycotoxin-producing fungus *Fusarium graminearum*

Yunqing Jian [a], Xia Chen [a], Temoor Ahmed [a], Qinghua Shang [a], Shuai Zhang [b], Zhonghua Ma [a], Yanni Yin [a,*]

[a] *State Key Laboratory of Rice Biology, Institute of Biotechnology, Zhejiang University, Hangzhou 310058, China*
[b] *National Agro-technology Extension and Service Center, Beijing 100125, China*

HIGHLIGHTS

- AgNPs possess high activity towards fungicide-resistant strains.
- AgNPs exert great activity against mycotoxin-producing fungus *F. graminearum*.
- AgNPs induce the expression of two azole resistance-related ABC genes.
- AgNPs lead to accumulation of toxisome and notorious mycotoxin DON by provoking ROS.
- AgNPs combined with DON-reducing fungicides are recommended for FHB control.

GRAPHICAL ABSTRACT
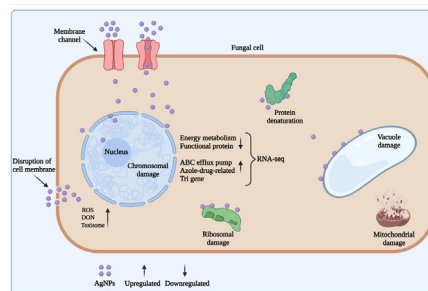
ARTICLE INFO

ABSTRACT

Introduction: Fusarium graminearum is a most destructive fungal pathogen that causes Fusarium head blight (FHB) disease in cereal crops, resulting in severe yield loss and mycotoxin contamination in food and feed. Silver nanoparticles (AgNPs) are extensively applied in multiple fields due to their strong antimicrobial activity and are considered alternatives to fungicides. However, the antifungal mechanisms and the effects of AgNPs on mycotoxin production have not been well characterized.

Objectives: This study aimed to investigate the antifungal activity and mechanisms of AgNPs against both fungicide-resistant and fungicide-sensitive *F. graminearum* strains, determine their effects on mycotoxin deoxynivalenol (DON) production, and evaluate the potential of AgNPs for FHB management in the field.

Methods: Scanning electron microscopy (SEM), transmission electron microscopy (TEM), and fluorescence microscopy were used to examine the fungal morphological changes caused by AgNPs. In addition, RNA-Seq, qRT-PCR, and western blotting were conducted to detect gene transcription and DON levels.

Results: AgNPs with a diameter of 2 nm exhibited effective antifungal activity against both fungicide-sensitive and fungicide-resistant strains of *F. graminearum*. Further studies showed that AgNP application could impair the development, cell structure, cellular energy utilization, and metabolism pathways of this fungus. RNA-Seq analysis and sensitivity determination revealed that AgNP treatment significantly induced the expression of azole-related ATP-binding cassette (ABC) transporters without compromising the control efficacy of azoles in *F. graminearum*. AgNP treatment stimulated the generation of reactive oxygen species (ROS), subsequently induced transcription of DON biosynthesis genes, toxisome formation, and mycotoxin production.

Conclusion: This study revealed the underlying mechanisms of AgNPs against *F. graminearum*, determined their effects on DON production, and evaluated the potential of AgNPs for controlling

Peer review under responsibility of Cairo University.

* Corresponding author.
  E-mail address: ynyin@zju.edu.cn (Y. Yin).

fungicide-resistant *F. graminearum* strains. Together, our findings suggest that combinations of AgNPs with DON-reducing fungicides could be used for the management of FHB in the future.

Introduction

Recently, with the rapid development of nanotechnology, engineered nanomaterials have been developed as antimicrobial agents to manage agricultural diseases owing to their strong antimicrobial activity [1–3]. Among all the nanoparticles characterized, silver nanoparticles (AgNPs) have gained significant attention due to their unique physicochemical properties e.g. cost-efficiency, higher stability, large surface/mass ratio, minimum toxicity and high reaction rate [4,5]. Approximately 320 tons of AgNPs are produced annually, and AgNPs are being widely applied in the medical and agricultural fields [6]. Moreover, studies have shown that micromolar doses of AgNPs are sufficient to kill microbial pathogens [7,8]. AgNPs have been reported to exhibit strong antifungal activity against a wide range of bacterial [9] and fungal pathogens, including *Aspergillus niger* [10], *Fusarium* spp. [11], *Candida* [12], *Raffaelea* sp. [13], *Pythium aphanidermatum*, *Sclerotinia sclerotiorum*, and *Macrophomina phaseolina* [14]. However, studies of this nanomaterial against mycotoxin-producing phytopathogenic fungi are limited, and the effect of AgNPs on deleterious mycotoxin biosynthesis remains unclear.

According to available literature, AgNPs exert antimicrobial activity by adhering to the surface of cell wall and membrane, penetrating cells, damaging intracellular structures, inducing the production of cellular toxicity and oxidative stress, and modulating the signal transduction pathways [15,16]. It is noteworthy that AgNPs can target distinct substrates and exhibit antimicrobial activity against multidrug resistance (MDR) microbes. The application of AgNPs in controlling MDR microbes has been extensively studied in bacteria and an emergent multidrug-resistant yeast *Candida auris* [17,18]. However, relevant studies on fungicide-resistant phytopathogenic fungi are insufficient, and the molecular mechanisms of AgNPs against pathogenic microbes have not yet been fully elucidated.

Fusarium graminearum is a major causal agent of Fusarium head blight (FHB), which leads to great economic losses on wheat, barley, maize, and other important cereal crops [19]. During the infection process and warehousing period, *F. graminearum* can produce various mycotoxins, particularly trichothecene deoxynivalenol (DON), which is detrimental to human and animal health [19]. Due to the lack of wheat cultivars with high resistance to *F. graminearum*, chemical fungicides are still the most effective method to manage FHB [20]. However, with the frequent and long-term use of fungicides, the emergence of fungicide-resistant *F. graminearum* populations in the field has significantly reduced the control efficiency and limited application of fungicides [21]. For example, carbendazim cannot effectively prevent FHB in the field owing to the high occurrence of carbendazim-resistant *F. graminearum* populations, which is accompanied by an increase in DON production [22]. Recent studies have demonstrated that the application of some commonly used azole fungicides (epoxiconazole, propiconazole, and tebuconazole) and QoI azoxystrobin can induce DON production [21]. To circumvent this predicament, new antifungal agents should be explored and investigated. Several studies have shown that nanoparticles, including graphene oxide-silver nanocomposite, chitosan, zinc oxide, and green or engineered silver nanoparticles, can exert decent antifungal effects against *F. graminearum* [1,23,24]. However, the molecular mechanisms of these nanomaterials against *F. graminearum* and the effects of

nanomaterial application on DON biosynthesis remain largely unknown. In literature, there are few studies on the application of nanoparticles against fungicide-resistant and mycotoxin-producing fungi [11,18]. Therefore, it is necessary to evaluate the potential risks of using nanoparticles for plant disease control.

This study aimed to systematically investigate the antifungal activity and toxicity mechanisms of AgNPs against the FHB pathogen *F. graminearum* using scanning electron microscopy (SEM), transmission electron microscopy (TEM), fluorescence microscopy, and RNA sequencing and explore their effects on DON production using qRT-PCR and western blot analysis. This study will advance the understanding of nanomaterial applications for plant disease control.

Materials and Methods

Strains and sensitivity determination

The wild-type PH-1 strain (NRRL 31084) of *F. graminearum* was used as the parental strain. Mycelial growth of the PH-1 and ABC deletion mutants was assessed on potato dextrose agar (PDA) (200 g potato, 20 g glucose, 10 g agar, and 1 L water) with or without AgNPs (N196423, Sigma, MO, USA), 0.25 µg/ml tebuconazole, 1 µg/ml difenoconazole or 1 µg/ml diniconazole. After incubation at 25 °C for 2 or 3 days, the colony diameter on each plate was measured in two perpendicular directions, with the original mycelial plug diameter (5 mm) subtracted from each measurement. For each plate, the average colony diameter was used for calculating mycelial growth inhibition. Each experiment was repeated twice, and each concentration included three replicates.

After the inoculation of PH-1 on PDA media containing serial dilutions of AgNPs (2 nm) (0, 1, 1.5, 2, 3, 6, 8, and 10 µg/ml), the plates were incubated at 25 °C for 2 days. After that, colony diameter and mycelial growth inhibition were measured and calculated as described above. The EC_{50} and EC_{90} values (effective concentrations that resulted in 50% and 90% mycelial growth inhibition, respectively) were calculated using the data processing system (DPS) computer program (Hangzhou Reifeng Information Technology Ltd., Hangzhou, China). As the two experiments did not differ significantly ($P > 0.05$, Fisher's least significant difference test), the two experiments' average EC_{50} and EC_{90} values were used in data analysis.

Conidiation and conidium germination tests

To assess the effect of AgNPs on *F. graminearum* conidiation, six fresh mycelial plugs of PH-1 were inoculated in a 50 ml flask containing 30 ml of carboxymethylcellulose (CMC) broth (1 g NH_4NO_3, 1 g KH_2PO_4, 0.5 g $MgSO_4 \cdot 7H_2O$, 1 g yeast extract, 15 g CMC, and 1 L water) [25]. The flasks were incubated at 25 °C with constant shaking at 180 rpm on a shaker. After 24 h of incubation, AgNPs were added to each flask to final concentrations of 0 µg/ml, 1 µg/ml, 1.88 µg/ml (EC_{50}), and 5.15 µg/ml (EC_{90}) and incubated for another 3 days. Subsequently, the conidia in each flask were filtered, and the number of conidia was determined using a hemocytometer. Furthermore, conidium germination was examined after fresh conidia were incubated at 25 °C in 2% sucrose water. Each experiment was repeated twice, and each concentration included three replicates.

Gene deletion and construction of GFP fusion cassettes

The double-joint PCR approach [26] was used to generate gene replacement constructs for the target genes *FgSTOA*, *FgFLOA*, and *FgTRI1*. The 5′ and 3′ flanking regions of each gene were amplified with the primer pairs listed in Table S1. After that, the amplified sequences were fused with the hygromycin resistance gene cassette (*HPH*). Protoplast transformation of *F. graminearum* was performed using a polyethylene glycol (PEG)-mediated protoplast transformation method as described previously [27].

To construct the FgStoA-GFP (green fluorescent protein) cassette, the FgStoA-GFP fusion fragment was transformed with XhoI-digested pYF11 into the yeast strain XK1-25 using the Alkali-Cation^{TM} Yeast Transformation Kit (MP Biomedicals, Solon, USA) to generate the FgStoA-GFP fusion vector. FgFloA-GFP and FgTri1-GFP fusion cassettes were constructed by using a similar strategy. The FgStoA-, FgFloA-, and FgTri1-GFP vectors were transformed into the deletion mutants ΔFgStoA, ΔFgFloA, and ΔFgTri1, respectively. Geneticin (*G418*) was used as the second selectable marker. All mutants generated in this study were preserved in 20% glycerol at −80 °C.

Staining and microscopic examination

The effect of AgNPs on the cell membranes of *F. graminearum* mycelia were analyzed using the FM4-64 (T13320, Invitrogen) staining method as described previously [28]. Briefly, the treated mycelia were immersed in FM4-64 solution (7.5 μM) at room temperature for 5 min and the stained mycelia were examined under a Zeiss LSM780 confocal microscope (Gottingen, Niedersachsen, Germany). The complementary strains bearing FgStoA-GFP or FgFloA-GFP were treated with or without AgNPs for 4 h and then observed at excitation and emission wavelengths of 488 and 525 nm, respectively, under a Zeiss LSM780 confocal microscope.

Morphological observation of F. graminearum via SEM and TEM

To observe the cellular alterations in *F. graminearum* caused by AgNPs, cell morphology was examined using scanning electron microscopy (SEM, TM-1000, Hitachi, Japan) and transmission electron microscopy (TEM, JEM 1230, JEOL, Akishima, Japan). The mycelia of PH-1 were treated with AgNPs at concentrations of 0, 1.88 μg/ml (EC$_{50}$) and 5.15 μg/ml (EC$_{90}$) at 25 °C and 180 rpm for 2 h. Thereafter, the mycelia of each sample were washed thrice with PBS and immersed in glutaraldehyde (2.5% [v/v]) overnight. The samples were post-fixed in osmium tetroxide (1% [w/v]) for 2 h at room temperature and dehydrated using a concentration gradient of ethanol (30 %-100%) until they were fully dehydrated. Finally, the morphological changes in *F. graminearum* were observed via SEM and TEM.

Sample preparation for RNA-Seq and bioinformatic analysis

Six mycelial plugs of the wild-type strain PH-1 were prepared in 200 ml liquid YEPD media, and the cultures were incubated at 25 °C and 180 rpm in a shaker. After 36 h, an AgNP solution was added to the cultures to a final concentration of 1.88 μg/ml (the EC$_{50}$ value). The control and AgNP-treated samples were harvested after incubation for 2 h, immediately frozen in liquid nitrogen, and then stored at −80 °C for RNA-Seq (RNA-Sequencing) analysis.

Total RNA was extracted using RNA Prep Pure Kit DP432 (TIANGEN Biotech Co., Ltd., Beijing, China) following the manufacturer's instructions. All RNA samples were assessed for integrity using the Qsep1 instrument. RNA libraries were constructed with the MGIEasy mRNA Library Prep Kit using 3 μg of total RNA. The procedure included polyA-selected RNA extraction, RNA fragmenta-

tion, random hexamer-primed reverse transcription, and 100 nt paired-end sequencing with MGI 2000.

Cutadapt (version 1.11) was used to filter the adapters and low-quality reads. Only two mismatches were allowed when clean reads were mapped to the *F. graminearum* reference transcripts using Hisat2 (version 2.1.0). These genes were subjected to alignment against the public protein databases Pfam (Pfam Protein families) and Uniprot (Swiss-Prot). It comprised RSEM (v1.2.6) for transcript abundance estimation and normalization of expression values as fragments per kilobase of transcript per million fragments mapped (FPKM). Differentially expressed genes were identified using DESeq2 with a filter threshold of adjusted q-value < 0.05 and |log2FoldChange| > 1. ClusterProfiler (http://www.bioconductor.org/packages/release/bioc/html/clusterProfiler.html) in the R package was used to perform the GO and Kyoto Encyclopedia of Genes and Genomes (KEGG) enrichment analyses. The GO and KEGG enrichment analyses were performed using a hypergeometric distribution with a Q value cutoff of 0.05. Q values obtained via Fisher's exact test were adjusted with FDR for multiple comparisons.

RNA preparation and quantitative reverse transcription PCR (qRT-PCR)

Samples were incubated for 36 h at 25 °C and 180 rpm, and AgNPs were added to the cultures at final concentrations equal to the EC$_{50}$ and EC$_{90}$. Treatments without AgNPs were used as controls. After incubation for an additional 2 h, the mycelia were used for total RNA extraction using TRIzol (TaKaRa Biotechnology, Dalian, China) according to the manufacturer's instructions. The reverse cDNA transcripts were synthesized using a HiScript II 1st Strand cDNA Synthesis Kit (Vazyme Biotech, Nanjing, China) to detect the transcription of each gene. The expression levels of six *TRI* genes and 14 *ABC* transporter genes were determined with qRT-PCR using HiScript II Q RT SuperMix (Vazyme Biotech, Nanjing, China), and the *FgACTIN* gene was used as the endogenous control. The primers used for qRT-PCR assays are listed in Table S1. The relative expression levels of target genes were calculated using the 2$^{-ΔΔCt}$ method [29]. The experiments were performed in independent biological triplicates.

Synergistic interactions between AgNPs and tebuconazole

To determine whether the induction of ABC transporters by AgNPs affects the efficacy of tebuconazole, following three mixture ratios were prepared: AgNPs: tebuconazole = 2:1, AgNPs: tebuconazole = 1:1, and AgNPs: tebuconazole = 1:2. Thereafter, the mixtures were diluted with PDA medium to concentrations of 0.096, 0.192, 0.384, 0.768, 1.536, 3.072, and 6.144 μg/ml. The toxicities of the mixtures against *F. graminearum* were determined using the mycelial growth rate method [30].

The inhibition rate was converted into a probability value, and the concentration was converts into a natural logarithm [31]; then, the probability value of the inhibition rate was assumed as "y" and the natural logarithm of the concentration as "x" and the virulence regression equation was calculated, followed by the calculation of the EC$_{50}$ value of each mixture. To determine the synergistic interactions of the mixtures, Wadley's model was used to calculate the theoretical EC$_{50}$ (EC$_{50th}$); the EC$_{50th}$ values were calculated according to the following equation [32]:

$$EC_{50th} = (a + b) / [a / EC_{50} (A) + b / EC_{50} (B)]$$

Where "a" is the concentration of A in a mixture and "b" is the concentration of B in a mixture. EC$_{50}$ (A) is the observed EC$_{50}$ value of A, and EC$_{50}$ (B) is the observed EC$_{50}$ value of B.

The EC$_{50ob}$ value was estimated via linear regression of the probit-transformed relative inhibition value (1-RG) at the log10

transformed-mixture concentration. The interaction level (R) of the mixtures was determined using the following equation:

$$R = EC_{50th} / EC_{50ob}$$

The synergistic interaction of mixtures was defined as synergistic when $R > 1.5$, additive when $1.5 > R > 0.5$, and antagonistic when $R < 0.5$.

DON production assays

To quantify DON production, PH-1 strain was grown in the toxin biosynthesis inducing (TBI) medium for 24 h at 28 °C. Thereafter, the AgNPs were added and the culture was incubated for an additional 6 days, with constant shaking at 150 rpm, in the dark. To quantify DON production in each sample, the DON quantification kit Wis008 (Wise Science, Zhenjiang, China) was used. Each experiment was conducted in triplicate.

Toxisome induction and western blot assays

To observe toxisome formation, 25 µl mycelia of the FgTri1-GFP labeled strain were added to 25 ml TBI medium. After incubation for 24 h at 28 °C and 150 rpm in the dark, AgNPs were added to each flask to generate final concentrations of 1 µg/ml, 1.88 µg/ml (EC_{50}), and 5.15 µg/ml (EC_{90}) and incubated for another 24 h. Treatments without AgNPs were used as controls. The FgTri1-GFP marker indicated toxisome formation and was observed under a Zeiss LSM780 confocal microscope (Gottingen, Niedersachsen, Germany).

The corresponding protein levels of each sample bearing FgTri1-GFP were detected via western blotting. Briefly, ∼500 mg of freshly prepared mycelia from each sample were finely ground in liquid nitrogen. The powder of each ground sample was suspended in 1 ml of extraction buffer. The lysates were homogenized with a vortex shaker and then centrifuged at 4 °C and 10, 000 *g* for 20 min. The resulting supernatants were analyzed via western blotting with a monoclonal anti-GFP (ab32146, Abcam, Cambridge, UK, 1:5000 dilution) antibody. Samples detected with a monoclonal anti-GAPDH antibody (EM1101, Hua An Biotech. Ltd., Hangzhou, China, 1:5000 dilution) were used as the reference. Each experiment was conducted in triplicate.

ROS staining and observation

To assess ROS production under TBI conditions, fungal hyphae incubated for 24 h and then treated with or without AgNPs for another 48 h were stained with 10 µM DCFH-DA (S0033S, Beyotime, Shanghai, China). Hyphae were stained with DCFH-DA dye at room temperature for 30 min and then observed in a bight/fluorescence field of view at the excitation and emission wavelengths of 488 and 525 nm, respectively, under a Zeiss LSM780 confocal microscope (Gottingen). Each experiment was conducted in triplicate.

Results

Inhibition of growth and conidial development

Accumulating evidence has shown that AgNPs possess strong antimicrobial activity depending on their physical and chemical properties, particularly particle size [33]. To characterize the effect of particle size of AgNPs on *F. graminearum*, we collected three types of engineered AgNPs with diameters of 2, 15, and 60 nm. After that, we tested their activity against mycelial growth of the wild-type strain PH-1. As shown in Fig. 1A, mycelial growth was inhibited by all types of AgNPs. However, the antifungal activity

of AgNPs was dependent on particle size. AgNPs with a diameter of 2 nm displayed the highest antifungal activity, whereas those with a diameter of 60 nm showed the lowest inhibitory effect. Hence, 2 nm AgNPs were selected for further study. Furthermore, the EC_{50} and EC_{90} values, which are the effective concentrations of a fungicide that inhibit mycelial growth by 50% and 90% relative to the control, were calculated using a mycelial growth assay. The EC_{50} and EC_{90} were found to be 1.88 µg/ml and 5.15 µg/ml, respectively (Fig. 1B).

To determine the role of AgNPs in asexual development, six fresh mycelial plugs of PH-1 were inoculated in CMC liquid medium to induce conidiation. After 24 h of inoculation, 2 nm AgNPs at different concentrations were added to each flask for another 3-day-culture. The results showed that 2 nm AgNPs significantly inhibited conidial production (Fig. S1A). To further determine whether AgNPs disrupt the germination of conidia, we treated conidia with AgNPs and assessed their germination under a microscope. As shown in Fig. 1C, the growth of germ tubes was significantly suppressed even with 1 µg/ml AgNPs. Similarly, the conidium germination rate was also reduced with an increase in AgNP concentration (Fig. S1B). In summary, these results indicate that 2 nm AgNPs exhibit strong inhibitory activity against mycelial growth and asexual development of *F. graminearum*.

Antifungal activity against drug-resistant strains

While AgNPs have been extensively reported for controlling MDR bacteria and *C. auris* [17,18], whether they can be used to control phytopathogenic fungicide-resistant strains is largely unknown. To investigate whether AgNPs are also effective against the fungicide-resistant strains of *F. graminearum*, we determined the inhibitory effect of AgNPs against *F. graminearum* strains resistant to each of the six commonly used fungicides. Car^R, Teb^R, Pro^R, Flu^R, Phe^R, and Pyd^R are resistant to carbendazim, tebuconazole, prochloraz, fludioxonil, phenamacril, and pydiflumetofen, respectively. The wild type and the resistant strains were inoculated on PDA plates containing the corresponding fungicides or AgNPs. As shown in Fig. 1D, PH-1 strains were completely inhibited by all the tested fungicides, whereas the resistant strains grew normally on the corresponding fungicide-containing plates. However, the mycelial growth of all resistant strains was abolished on AgNP-containing plates, which is similar to the case in PH-1 (Fig. 1D). These results indicate that AgNPs have a decent antifungal activity against various fungicide-resistant strains of *F. graminearum*.

Effect of AgNPs on fungal morphology

The fungal cell wall is composed of glucan and chitin, which protect cells from environmental stimuli and impart host immunity [34]. Although their antimicrobial mechanisms are complicated, AgNPs are known to exert antimicrobial effects by damaging the membrane integrity and structure of cells [15,16]. Therefore, we stained the cell membrane with FM4-64, a type of amphiphilic styryl dye commonly used as a membrane-selective fluorescent dye. FM4-64 cannot enter intact cells via unfacilitated diffusion [35]. As shown in Fig. 2A, the intact plasma membrane and septa of wild-type hyphae were stained with FM4-64 without treatment with AgNPs. However, upon treatment with 1 µg/ml AgNPs, the FM4-64 dye began to enter the hyphal cells, and a partial fluorescence signal could be observed in the intracellular organelles, such as vacuoles and endosomes; however, most of the hyphae were still intact (Fig. 2A). Furthermore, when treated with AgNPs at EC_{50} or EC_{90} concentrations, the hyphae were significantly thinner than the untreated or low-concentration treated hyphae, which might be the consequence of cell membrane disruption and hyphae dehydration. In addition, no intact hyphae could
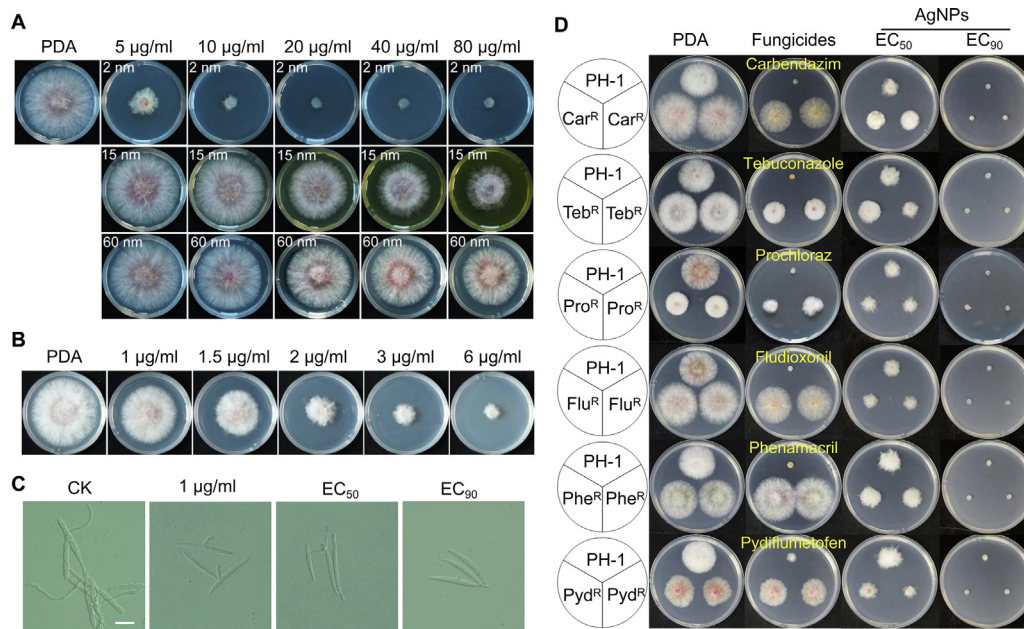
Fig. 1. AgNPs impair the growth and asexual development of *F. graminearum*. (A) AgNPs with different sizes and concentrations inhibited the mycelial growth of PH-1. Colony morphology of the wild-type strain PH-1 cultured on PDA with or without AgNPs at 25 °C for 2 days. (B) AgNPs with the diameter of 2 nm inhibited mycelia growth of *F. graminearum*. Colony morphology of PH-1 cultured on PDA with or without 2 nm AgNPs at 25 °C for 2 days. (C) AgNPs with the diameter of 2 nm disrupted conidium germination of *F. graminearum*. Differential interference contrast [DIC] images of germ tube were captured with an electronic microscope. EC_{50} = 1.88 μg/ml and EC_{90} = 5.15 μg/ml. (D) AgNPs display antifungal activity against various drug-resistant strains of *F. graminearum*. Five-mm mycelial plugs of each strain were inoculated on PDA plates supplemented with 5 μg/ml each fungicide, or AgNPs at the concentrations of EC_{50} (1.88 μg/ml) or EC_{90} (5.15 μg/ml), and then incubated at 25 °C for 2 days.

be observed in the field of view, and some of the hyphae even broke down during AgNP treatment (Fig. 2A).

To further elucidate the function of AgNPs on membrane, we first labeled two putative membrane marker proteins, FgFloA and FgStoA, with a green fluorescent protein (GFP). Both FloA and StoA localized along the plasma membrane and were thought to be good candidates for forming apical Sterol-Rich plasma membrane Domains (SRDs) [36]. Based on this data, GFP-tagged FgFloA-GFP and FgStoA-GFP were introduced into the ΔFgFloA and ΔFgStoA mutants to obtain FgFloA-GFP (ΔFgFloA::FgFloA-GFP) or FgStoA-GFP (ΔFgStoA::FgStoA-GFP)-expressing strain for further study. Microscopic observation showed that FgStoA-GFP localized as stable dots along the plasma membrane, whereas FgFloA mainly localized at the cortex of the plasma membrane before treatment
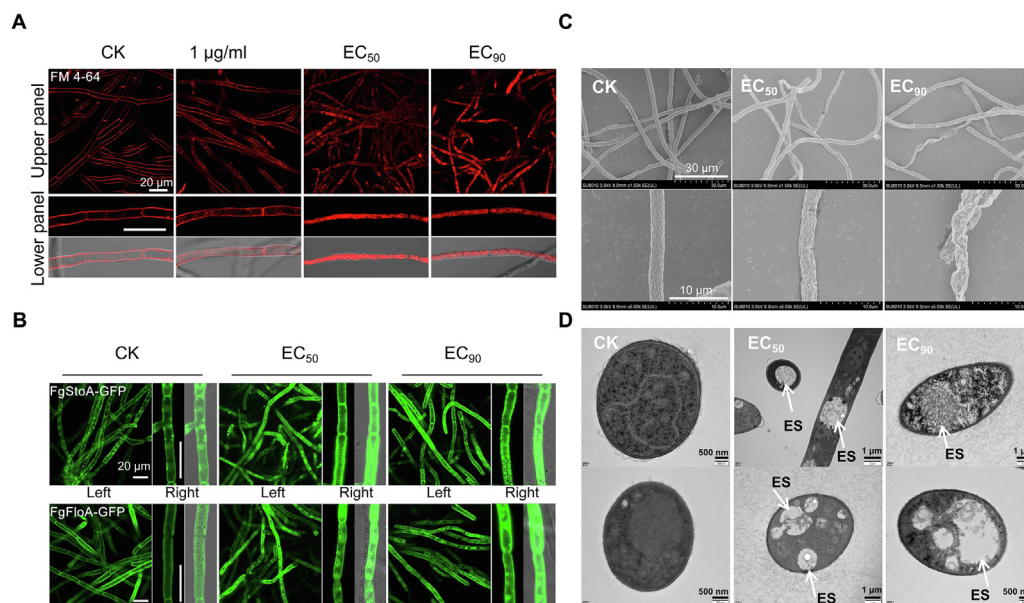

Fig. 2. AgNPs disrupt fungal morphology of *F. graminearum*. (A) Fluorescence images of PH-1 mycelia after staining with membrane-selective dye FM4-64, with or without AgNP treatment. EC_{50} = 1.88 μg/ml and EC_{90} = 5.15 μg/ml [Scale bar = 20 μm]. (B) Fluorescence images of two membrane marker proteins with or without AgNP treatment [Scale bar = 20 μm]. (C) SEM images of PH-1 mycelia observed after treating with or without AgNP treatment. EC_{50} = 1.88 μg/ml and EC_{90} = 5.15 μg/ml. Bars, upper panel = 30 μm, lower [Scale bar = 10 μm]. (D) TEM images of PH-1 mycelia were observed after treating with or without AgNPs. EC_{50} = 1.88 μg/ml and EC_{90} = 5.15 μg/ml. ES: empty spaces. Bars are indicated in each image.

(Fig. 2B). However, after treatment with AgNPs at EC_{50} or EC_{90} concentrations, both FgStoA and FgFloA localized along the plasma membrane and entered the fungal cells, where green fluorescence was detected (Fig. 2B), indicating that AgNPs may disrupt plasma membrane structure. After that, to eliminate the possibility of AgNPs damaging plant cell membranes, we evaluated the effect of AgNPs on wheat seed germination and found that AgNPs at EC_{50} and EC_{90} concentrations had no impact on germination rate and root growth (Fig. S1C).

SEM and TEM analyses were conducted to study the morphological changes in hyphae and fungal cells after treatment with AgNPs. SEM images showed external changes, which suggested that AgNP treatment led to disrupted hyphal structure and shrank hyphae as compared to that in the untreated group (CK) (Fig. 2C). Consistently, the analysis of intracellular changes observed via TEM revealed that the organelles were degraded by AgNPs, as empty spaces could be observed (Fig. 2D). Taken together, these results showed that AgNPs were toxic to *F. graminearum,* and both the surface and intracellular organelles of the fungal cell were disrupted.

KEGG analysis of the downregulated genes

To further elucidate the molecular mechanism of AgNPs against *F. graminearum*, we performed RNA-Seq analysis. The wild-type strain PH-1 was incubated in a yeast extract peptone dextrose (YEPD) medium with or without AgNPs at a concentration equal to EC_{50}. Among all differentially expressed genes, 3669 were upregulated and 3381 were downregulated in response to AgNP treatment (Fig. S2). Functional KEGG analysis of the downregulated genes revealed that treatment with AgNPs led to reduction in the biosynthesis of several amino acids and expression of metabolism pathways, including the phenylalanine, tyrosine, and tryptophan biosynthesis pathways, valine, leucine, and isoleucine biosynthesis pathways, and arginine, proline, methane metabolism, and alanine, aspartate, and glutamate metabolism pathways (Fig. 3; Table S2). Amino acids can be utilized for synthesis of proteins, peptides, and other nitrogen-containing substances. In addition, the α-keto acids generated from amino acids can be oxidized into carbon dioxide via the tricarboxylic acid cycle, which provides energy for living organisms [37]. In this study, AgNP treatment could repress N-glycan biosynthesis pathways (Fig. 3), which are used for glycosylation for protein folding, stability, and localization [38]. Together, these data suggest that AgNPs can affect cellular energy utilization processes and metabolism pathways, leading to their high activity.

KEGG analysis of the upregulated genes

Six significant (*P*-value < 0.05) pathways that were upregulated by AgNPs, compared to that in the untreated group, were also analyzed (Table S3). As shown in Fig. 4, several pathways involved in mismatch repair, nucleotide excision repair, and processes such as spliceosome and ribosome biogenesis and basal TF-mediated regulation of the most basic and core vital activity of gene expression were elevated by AgNPs. These data suggest that treatment with AgNPs might cause abnormal activities in the genome, thereby upregulating the expression of genes in the DNA damage response (DDR) and genetic central dogma. However, the expression levels of ABC transporters were also increased by AgNP treatment (Fig. 4; Table S3). We randomly selected several ABC transporter genes, based on our previous study [39] and RNA-Seq data, to perform qRT-PCR assays. As shown in Fig. 5A, expression levels of the 14 *FgABC* genes were increased to different degrees when treated with AgNPs for 1 or 2 h, indicating that ABC

transporters might be responsible for the detoxification of AgNPs. In addition, we determined the sensitivities of these 14 *FgABC* deletion mutants to AgNPs, which were obtained from a previous study [39]. However, these deletion mutants did not show significant differences in AgNP sensitivity compared to the wild type (Table S4), which may be due to the functional redundancy of FgABC transporters.

The ABC transporter family is known for its involvement in multidrug resistance and can utilize ATP to transport toxic compounds, inorganic ions, metals, peptides, steroids, nucleosides, sugars, and various other small molecules [39–41]. Our results showed that AgNPs can induce *FgABC* transcription; therefore, we investigated the effect of AgNPs on FgABC-mediated fungicide resistance in *F. graminearum*. We first determined the fungicide sensitivity of the 14 up-regulated FgABC deletion mutants and found that the single deletion mutants ΔFg08312 and the double deletion mutants ΔFg05527-08312 and ΔFg08312-05527 exhibited significantly increased sensitivity to all the tested azole fungicides, compared to the wild type (Fig. 5B and C; Table S4). In contrast, ΔFg05527 showed significant sensitivity to difenoconazole and tebuconazole, indicating that these two FgABC transporters are vital for the excretion of azoles. However, other FgABC transporters were not involved in the sensitivity to the 12 tested fungicides (Table S4). Based on these results, we explored whether the induction of *Fg05527* and *Fg08312* would decrease the control efficacy of azole fungicides. To test our hypothesis, we mixed AgNPs with tebuconazole, the most widely applied azole fungicide to control FHB, and calculated the interaction level (R) of the mixtures. The synergistic interactions of the three blending ratios are listed in Table 1. However, all three mixture ratios showed additive effects, suggesting that the antifungal efficacy of azoles will not be compromised by the ABC efflux pump enhanced by AgNPs.

Upregulation of DON biosynthesis genes

DON is the primary mycotoxin produced by *F. graminearum* during pathogenesis, and its biosynthesis is regulated by 15 trichothecene biosynthesis genes (*FgTRIs*) [42]. Owing to the threat of DON to human and animal health, the control efficiency of DON contamination is considered a critical indicator to evaluate and apply fungicides for the management of FHB [43]. To study the relationship between AgNPs and DON production, we first determined DON production in response to AgNP treatment. As shown in Fig. 6A, DON production was significantly increased after treatment with AgNPs compared to that in the control. Furthermore, qRT-PCR assays were conducted to determine the transcription levels of six *FgTRI* genes, namely, *FgTRI1*, *FgTRI4*, *FgTRI5*, *FgTRI6*, *FgTRI12*, and *FgTRI101*. Consistently, all six *FgTRI* genes were significantly upregulated in response to AgNP treatment (Fig. 6B).

Induction of toxisome formation

Recently, *Fusarium* toxisomes have been assumed to be novel structures that harbor the DON biosynthesis enzyme and may indicate DON biosynthesis ability in *F. graminearum* [19]. Among the six AgNP-induced *FgTRI* genes, *FgTRI1* encodes a calonectrin oxygenase FgTri1, which catalyzes the late step in DON biosynthesis and is delivered to the toxisome under DON induction conditions. Therefore, the formation of toxisomes can be reflected by FgTri1, which shows a positive correlation with DON production [42]. To characterize the subcellular localization of FgTri1 under AgNP treatment, *FgTRI1-GFP* was introduced into the FgTri1 mutant ΔFgTri1 to obtain FgTri1-GFP expressing strain (ΔFgTri1::FgTri1-GFP) for the toxisome induction assay. Under non-treatment con-
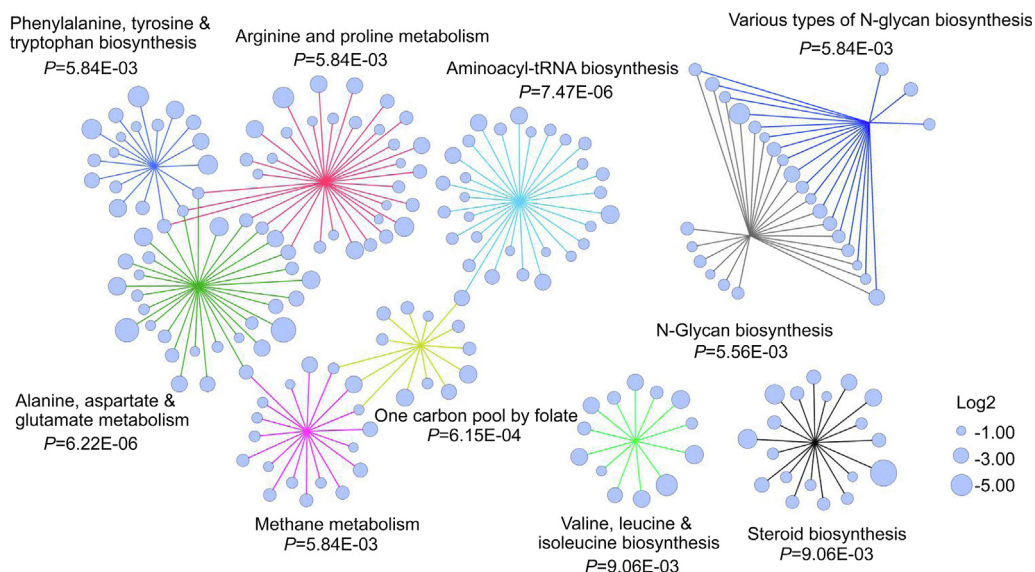
Fig. 3. KEGG analysis of down-regulated genes by AgNP treatment. Network analysis of the relationship between significantly down-regulated genes and the corresponding enriched KEGG pathways. The cyan circle indicated different gene. Involvement of these genes in different pathways was visualized with coloured lines representing each pathway. The relative fold change (log2-transformed) of gene expression is indicated by the circle size.

Fig. 4. KEGG analysis of up-regulated genes by AgNP treatment. Network analysis of the relationship between significantly up-regulated genes and the corresponding enriched KEGG pathways. The cyan circle indicated different gene. Involvement of these genes in different pathways was visualized with coloured lines representing each pathway. The relative fold change (log2-transformed) of gene expression is indicated by the circle size.
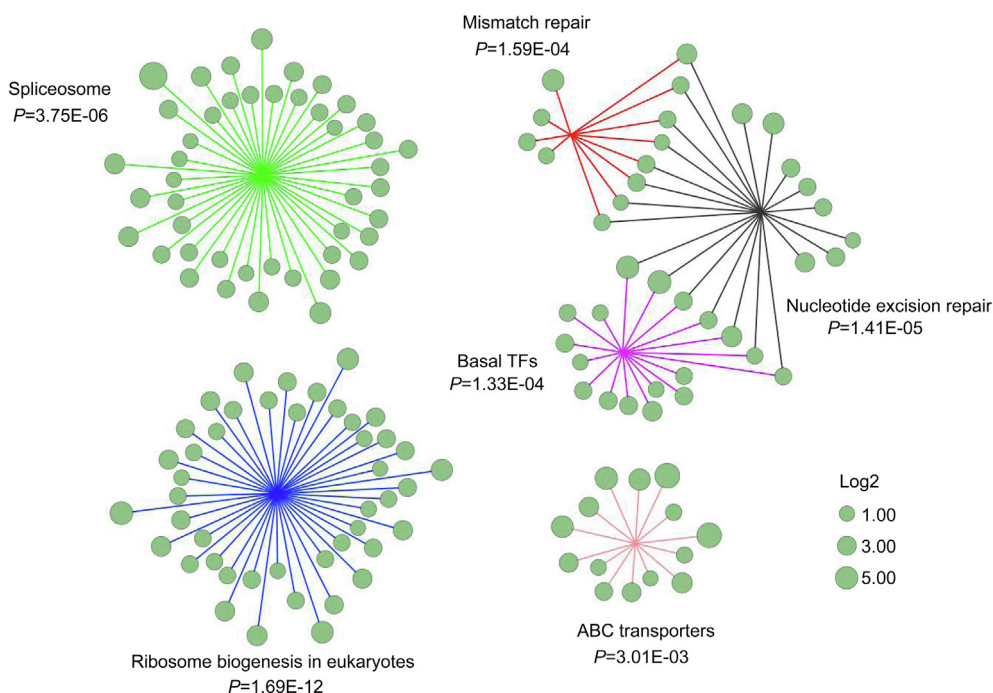
ditions, FgTri1-GFP was induced, and toxisomes were observed after incubation in TBI media for 48 h. After treatment with AgNPs, even at a low concentration (1 μg/ml), the fluorescence signals were significantly increased unexpectedly (Fig. 6C). Accordingly, the quantity of toxisomes significantly increased per unit length of hyphae (Fig. 6D). The protein content of FgTri1-GFP under different conditions was further verified via immunoblot assays using an anti-GFP antibody, and the results were consistent with the microscopic observations. As shown in Fig. 6E, the intensity of the FgTri1-GFP protein increased under AgNP treatment. In summary, these results indicate toxisome formation in *F. graminearum*.

Provoking of ROS

Induction of reactive oxygen species (ROS) and free radicals is one of the most important toxicity mechanisms of AgNPs [44]. Additionally, various studies have demonstrated that H_2O_2 production is highly correlated with the kinetics of DON accumulation in *F. graminearum* [45], which prompted us to speculate that AgNP-induced DON biosynthesis may result from ROS production. Therefore, we determined the ROS content of mycelia in PDB and TBI with or without AgNPs using fluorescent probes 2, 7-dichloro-dihydrofluorescein diacetate (DCFH-DA). There was a faint green flu-
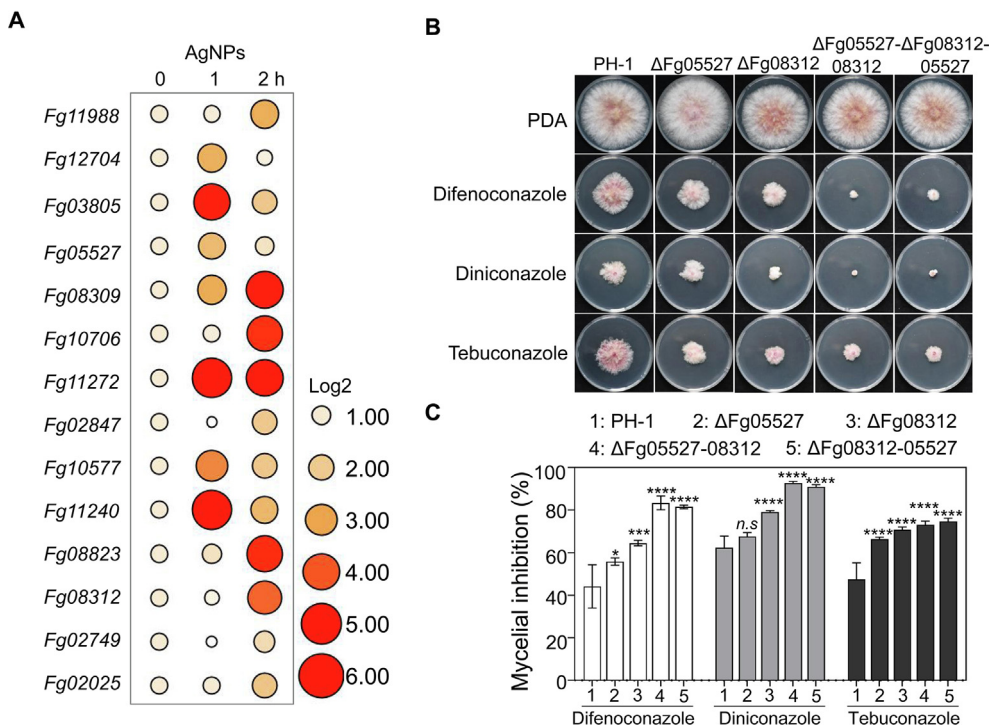
Fig. 5. AgNPs induce the transcription of azole sensitivity related ABC transporter genes. (A) ABC transporter genes were up-regulated upon AgNP treatment. The wild-type strain PH-1 was treated with AgNPs at EC_{50} for the indicated time, and the relative *ABC* expression normalized to *ACTIN* was analyzed with qRT-PCR. Means (n = 3) of fold induction compared to non-treatment shown as log2 values were used to construct heat-map using TBtools. The relative fold change (log2-transformed) of gene expression is indicated by the circle color and size. (B) Single and double deletion mutants of two ABC transporters show increased sensitivity to azole fungicides as compared with the wild type. Five-mm mycelial plugs of each strain were inoculated on PDA plates supplemented with 0.25 μg/ml tebuconazole, 1 μg/ml difenoconazole or 1 μg/ml diniconazloe incubated for three days at 25 °C. (C) Percentage of mycelial inhibition was calculated for each treatment. Means and standard errors were calculated from three repeated experiments. Significance was measured based on one-way ANOVA analysis (**** $P < 0.01$).

Table 1
The synergistic interactions of AgNPs and tebuconazole against *F. graminearum*.

AgNPs:Teb	EC_{50ob}(μg/ml)[a]	EC_{50th} (μg/ml)[b]	Virulence regression equation	R^2	Interaction level (R)	Synergistic interactions
2:1	0.5458	0.5924	y = 47.596x + 62.515	0.9326	1.0853	additive
1:1	0.4525	0.4413	y = 42.539x + 64.651	0.9201	0.9753	additive
1:2	0.2562	0.3516	y = 42.169x + 74.943	0.9582	1.3726	additive

Note: [a]EC_{50ob} value is the observed EC_{50}, which was estimated by the linear regression of the probit-transformed relative inhibition value (1-RG) at the log10 transformed-mixture concentration.
[b] EC_{50th} value is the theoretical EC_{50}, which was calculated following Wadley's model.

orescence of DCF in PDB, whereas in TBI, the fluorescence significantly increased (Fig. 6F), indicating that DON induction stimulates ROS generation. To further detect the effect of AgNPs on ROS induction, we used a TBI medium supplemented with AgNPs. As shown in Fig. 6F, ROS production in mycelia treated with AgNPs significantly increased compared to non-treated mycelia. To further confirm that ROS may trigger DON biosynthesis, qRT-PCR assays were conducted to detect the transcription levels of *FgTRI* genes after treatment with H_2O_2, a type of reactive oxidative species. Results showed that the transcription levels of *FgTRIs* were significantly upregulated (Fig. S3), which confirmed that AgNPs induced *FgTRI* expression by elevating ROS content. Together, these results indicate that AgNPs may induce DON production by promoting ROS generation.

Discussion

Given the increasing prevalence of drug- or antibiotic-resistant pathogenic microorganisms, further studies are needed to develop new antimicrobial materials to manage pathogen-borne diseases

[46]. The small size and large surface area to mass ratio confer nanoparticles with distinct physical, chemical, and biological properties compared to traditional antibiotics and fungicides [33]. Among various nanomaterials, AgNPs have been reported to be the most effective against multiple clinical as well as agricultural pathogens; accordingly, they have attracted significant attention for their ability to control MDR [47]. AgNPs have been used to combat MDR strains of several clinical pathogenic bacteria because of their broad-spectrum antimicrobial activity [48,49]. The green synthesis of AgNPs exhibited promising antibacterial activity against the agricultural pathogen *Enterobacter hormaechei* subsp. *hormaechei* strain ASE, which is resistant to various types of cell wall synthesis-, nucleic acid synthesis-, and protein synthesis-inhibiting antibiotics [50]. Although accumulating evidence has shown that AgNPs possess excellent antifungal activities against *Aspergillus*, *Candida*, *Fusarium*, *Phoma*, *Magnaporthe oryzae*, and *Trichoderma* [51–53], the activities of AgNPs against fungicide-resistant fungal strains are largely obscure. To our knowledge, this is the first study to report that AgNPs are highly effective against both fungicide-resistant and fungicide-sensitive *F. graminearum* strains.
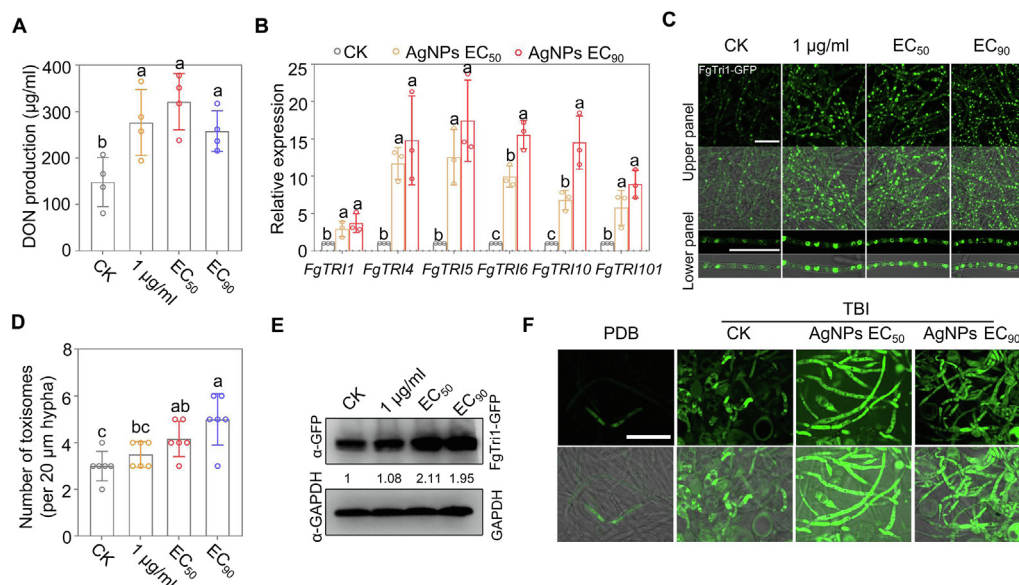
Fig. 6. AgNPs stimulate toxisome formation and DON production by provoking ROS. (A) AgNPs promoted DON accumulation in TBI. Each strain was treated with 1, 1.88 (EC_{50}) or 5.15 (EC_{90}) µg/ml AgNPs after 24-h-culture in TBI, then incubated for additional 6 days at 28 °C. Means and standard errors were calculated from three repeated experiments. Different letters represent statistically significant differences according to the one-way ANOVA test ($P < 0.05$). (B) The expression of *FgTRI* genes were induced by the treatment of AgNPs. Each strain was treated with 1 µg/ml, EC_{50} or EC_{90} AgNPs after 24-h-culture in TBI, then incubated for additional 48 h at 28 °C. The *FgACTIN* gene was used as internal control. Means and standard errors were calculated from three repeated experiments. Different letters represent statistically significant differences according to the one-way ANOVA test ($P < 0.05$). (C) AgNPs accelerated toxisome formation. After ΔFgTri1::FgTri1-GFP strain were cultured for 24 h at 28 °C, AgNPs was added to the cultures to final concentrations of 1 µg/ml, EC_{50} and EC_{90} values, respectively. After incubated for additional 24 h, the fluorescence signal of ΔFgTri1::FgTri1-GFP was examined [Scale bar = 40 µm]. (D) The average number of toxisomes in per 20 µm hypha. Samples were prepared as in (C). Means and standard errors were calculated from three repeated experiments. Different letters represent statistically significant differences according to the one-way ANOVA test ($P < 0.05$). (E) FgTri1-GFP protein levels were increased by AgNPs. The protein content of FgTri1-GFP was determined using an anti-GFP antibody by immunoblot assays. The anti-GAPDH was used as a control antibody. (F) AgNPs induce ROS generation in TBI medium. The wild-type strain PH-1 was cultured in PDB or TBI for 24 h. AgNPs were added to the cultures in TBI to final concentrations of EC_{50} (1.88 µg/ml) or EC_{90} (5.15 µg/ml) values, respectively. After incubated for additional 48 h, ROS production was determined using fluorescent probes 2, 7-dichlorodi-hydrofluorescein diacetate (DCFH-DA) [Scale bar = 50 µm].

This study found that 2 nm AgNPs exerted more efficient antifungal activity against *F. graminearum* than the 15 and 60 nm AgNPs (Fig. 1A). Several reports have demonstrated that AgNPs with smaller sizes display greater toxicity due to a higher surface area to mass ratio [54], which supports our results. Ibrahim et al. found that green-synthesized AgNPs inhibit conidium germination and germ tube growth in *F. graminearum* [23]. In addition, spore formation or germination inhibition has been observed in various other phytopathogenic fungi [55–58]. We found that engineered AgNPs inhibited conidium germination and germ tube formation and significantly reduced conidial production (Fig. 1C; Fig. S1A). These results indicate that AgNPs can effectively impede the asexual development of phytopathogenic fungi. Regarding the action mechanism of AgNPs, our work and studies in other bacteria and fungi all showed that AgNP application can disrupt the integrity and permeability of cell membranes [23,44] (Fig. 2). Moreover, the RNA-Seq data showed that AgNPs can reduce the transcription of genes related to cellular energy utilization and substance metabolism by KEGG category in *F. graminearum* (Fig. 3; Table S2). In another *Fusarium* fungus, similar findings have been reported recently [59], suggesting that disruption of cellular energy utilization and metabolism pathways are important components of the antifungal activity of AgNPs.

Several studies have shown that AgNP-induced toxicity can alter the activity of ABC transporters [31,60]. In enterobacterial pathogens, exposure to AgNPs significantly increased the transcription of ABC efflux pump proteins AcrA and AcrB [48]. Controversially, several reports on cancer cells have shown that both organic and inorganic nanoparticles can inhibit the functions of

ABC transporters to overcome cancer MDR [31,61]. In humans, the expression of ABC transporters is altered by AgNP-induced toxicity, a risk factor for neurodegenerative diseases [60]. Although deletion of FgABC transporters did not alter the sensitivity to AgNPs (Table S4), the expression levels of 14 FgABC transporters were induced by treatment with this nanomaterial (Fig. 5A), which is consistent with the results reported in enterobacteria [48]. In summary, AgNP treatment can affect the expression or function of ABC transporters, which might be conserved from prokaryotic to eukaryotic organisms. Given that ABC transporters function primarily via transporting compounds across cellular membranes [39], we deduce that the misregulation of ABC transporters caused by AgNPs might result from cell membrane disruption.

ABC transporter-mediated drug export is an important drug resistance mechanism [62]. In mammals, the overexpression of some ABC transporters causes resistance of cancer and tumor cells to anticancer drugs, which consequently results in chemotherapy failure [63]. Several ABC transporters have also been reported to contribute to azole resistance in *Candida* and other filamentous fungi [64–66]. In this study, two *F. graminearum* ABC transporters were responsible for azole resistance (Fig. 5B and C), suggesting that *F. graminearum* ABC transporters have conserved functions in azole resistance. Although AgNPs induced the expression of azole resistance-related ABC transporters (Fig. 5A), the antifungal efficacy of azoles was not compromised (Table 1). This phenomenon might be due to the complexity of azole resistance mechanisms; typically, the overexpression and point mutations of the target gene cytochrome P450 sterol 14α-demethylase (*CYP51*) play vital roles in regulating azole resistance in fungi [20]. Surprisingly,

we found that AgNPs conversely had additive effects on azole activity (Table 1). Previous studies have consistently revealed that AgNPs can synergistically work with a commercial antifungal agent, fluconazole, to exert their fungicidal effects against *C. albicans*, *F. semitectum*, *Phoma glomerata*, *P. herbarum*, and *Trichoderma* spp. [67,68]. We deduced that damage to the cell membrane caused by AgNPs may accelerate fungicide absorption, subsequently elevating the activity of fungicides. These results indicate that the mixture of AgNPs and some fungicides might increase the control efficacy of fungicides and reduce fungicide usage, ultimately contributing to fungicide resistance management.

Increasing evidence has shown that applying chemical fungicides at specific concentrations can induce DON production [21,69,70]. At present, fungicides that trigger DON biosynthesis in *F. graminearum* are of considerable concern. This study found that AgNPs with a diameter of 2 nm displayed strong antifungal activity against *F. graminearum* (Fig. 1), in addition to inducing DON biosynthesis (Fig. 6). Exposure to fullerol $C_{60}(OH)_{24}$ nanoparticles (FNP) showed great potential in reducing the concentrations of secondary metabolites in several fungi [71,72], which is different from our findings. Furthermore, we found that AgNP treatment stimulated DON production by promoting ROS generation (Fig. 6F; Fig. S3). Previous studies reported that ROS generation is a rapid response to general metal stress [6] and metal nanoparticles can also cause ROS-mediated genotoxicity [73]. Moreover, ROS has been highlighted as a stimulator of DON production in *F. graminearum* [45,74]. For example, ROS generated by the host increases DON production in *F. graminearum* during infection [45]. Similarly, exogenous supplementation with H_2O_2 directly increases DON production in *F. graminearum* [74]. These reports support our findings that AgNPs induced ROS production, resulting in DON accumulation in *F. graminearum* (Fig. 6). Together, our findings indicate that it is necessary to determine and balance the control efficiency and mycotoxin contamination when applying AgNPs against toxigenic fungi in the future.

Conclusion

Silver nanoparticles (AgNPs) exhibit excellent antifungal activity against fungicide-sensitive and fungicide-resistant *F. graminearum* strains via multiple action modes, including disruption of fungal development and cell membranes, perturbation of cellular energy utilization and metabolism pathways. Although AgNPs could cause the up-regulation of azole resistance-related ATP-binding cassette (ABC) transporter genes, the control efficacy of the fungicides was not altered. However, every coin has two sides: AgNPs display effective antifungal activity against *F. graminearum*, yet they can also increase the production of notorious mycotoxin deoxynivalenol (DON). Therefore, the antifungal activity and DON production caused by AgNPs need to be balanced before they can be used as effective and alternative therapeutic candidates for mycotoxin-producing pathogens. In conclusion, this study revealed that the combination of AgNPs with DON-reducing fungicides might be a choice for the management of Fusarium head blight (FHB) and can be used to develop fungicidal formulations. However, future studies are needed to evaluate the antimicrobial potential of AgNPs under realistic agricultural conditions.

CRediT authorship contribution statement

Yunqing Jian and **Yanni Yin:** Conceived, designed and performed the experiments; **Xia Chen** and **Qinghua Shang:** Performed the phenotype determination of ABC transporter deletion mutants; **Yunqing Jian, Xia Chen, Temoor Ahmed** and **Yanni Yin**: Analyzed the data; **Yunqing Jian, Temoor Ahmed, Shuai Zhang, Zhonghua Ma** and **Yanni Yin:** Wrote and revised the manuscript. All authors read and approved the manuscript.

Declaration of Competing Interest

The authors declare that they have no known competing financial interests or personal relationships that could have appeared to influence the work reported in this paper.

Compliance with Ethics Requirements
This article does not contain any studies with human or animal subjects.

Appendix A. Supplementary data

Supplementary data to this article can be found online at https://doi.org/10.1016/j.jare.2021.09.006.

References

[1] Chen J, Sun L, Cheng Y, Lu Z, Shao K, Li T, et al. Graphene oxide-silver nanocomposite: Novel agricultural antifungal agent against *Fusarium graminearum* for crop disease prevention. ACS Appl Mater Interfaces 2016;8 (36):24057–70. doi: https://doi.org/10.1021/acsami.6b0573010.1021/acsami.6b05730.s001.
[2] Hoseinzadeh E, Makhdoumi P, Taha P, Hossini H, Stelling J, Amjad Kamal M, et al. A review on nano-antimicrobials: Metal nanoparticles, methods and mechanisms. Curr Drug Metab 2017;18(2):120–8. doi: https://doi.org/10.2174/1389200217666161201111146.
[3] Li Q, Mahendra S, Lyon DY, Brunet L, Liga MV, Li D, et al. Antimicrobial nanomaterials for water disinfection and microbial control: Potential applications and implications. Water Res 2008;42(18):4591–602. doi: https://doi.org/10.1016/j.watres.2008.08.015.
[4] Siddiqi KS, Husen A, Rao RAK. A review on biosynthesis of silver nanoparticles and their biocidal properties. J Nanobiotechnol 2018;16:14. doi: https://doi.org/10.1186/s12951-018-0334-5.
[5] Pandian AMK, Karthikeyan C, Rajasimman M, Dinesh MG. Synthesis of silver nanoparticle and its application. Ecotoxicol Environ Saf 2015;121:211–7. doi: https://doi.org/10.1016/j.ecoenv.2015.03.039.
[6] Ahamed M, AlSalhi MS, Siddiqui MKJ. Silver nanoparticle applications and human health. Clin Chim Acta 2010;411(23-24):1841–8. doi: https://doi.org/10.1016/j.cca.2010.08.016.
[7] Liu Z, Stout JE, Tedesco L, Boldin M, Hwang C, Diven WF, et al. Controlled evaluation of copper-silver ionization in eradicating *Legionella pneumophila* from a hospital water distribution system. J Infect Dis 1994;169(4):919–22. doi: https://doi.org/10.1093/infdis/169.4.919.
[8] Rai M, Yadav A, Gade A. Silver nanoparticles as a new generation of antimicrobials. Biotechnol Adv 2009;27(1):76–83. doi: https://doi.org/10.1016/j.biotechadv.2008.09.002.
[9] Khezerlou A, Alizadeh-Sani M, Azizi-Lalabadi M, Ehsani A. Nanoparticles and their antimicrobial properties against pathogens including bacteria, fungi, parasites and viruses. Microb Pathog 2018;123:505–26. doi: https://doi.org/10.1016/j.micpath.2018.08.008.
[10] Xu Y, Gao C, Li X, He Yi, Zhou L, Pang G, et al. In vitro antifungal activity of silver nanoparticles against ocular pathogenic filamentous fungi. J Ocul Pharmacol Ther 2013;29(2):270–4. doi: https://doi.org/10.1089/jop.2012.0155.
[11] El-Naggar MA, Alrajhi AM, Fouda MM, Abdelkareem EM, Thabit TM, Bouqellah NA. Effect of silver nanoparticles on toxigenic Fusarium spp. and deoxynivalenol secretion in some grains. J AOAC Int 2018;101:1534–41. doi: https://doi.org/10.5740/jaoacint.17-0442.
[12] Xue B, He D, Gao S, Wang D, Yokoyama K, Wang L. Biosynthesis of silver nanoparticles by the fungus *Arthroderma fulvum* and its antifungal activity against genera of *Candida*. *Aspergillus* and *Fusarium*. Int J Nanomedicine 2016;11:1899–906. doi: https://doi.org/10.2147/IJN.S98339.
[13] Kim SW, Kim KS, Lamsal K, Kim YJ, Kim SB, Jung M, et al. An in vitro study of the antifungal effect of silver nanoparticles on oak wilt pathogen *Raffaelea* sp. J Microbiol Biotechnol 2009;19:760–4. doi: https://doi.org/10.4014/jmb.0812.649.

Y. Jian, X. Chen, T. Ahmed et al.

Journal of Advanced Research 38 (2022) 1–12

[14] Landarani-Isfahani A, Taheri-Kafrani A, Amini M, Mirkhani V, Moghadam M, Soozanipour A, et al. Xylanase immobilized on novel multifunctional hyperbranched polyglycerol-grafted magnetic nanoparticles: An efficient and robust biocatalyst. Langmuir 2015;31(33):9219–27. doi: https://doi.org/10.1021/acs.langmuir.5b02004.

[15] Durán N, Durán M, de Jesus MB, Seabra AB, Fávaro WJ, Nakazato G. Silver nanoparticles: A new view on mechanistic aspects on antimicrobial activity. Nanomedicine 2016;12(3):789–99. doi: https://doi.org/10.1016/j.nano.2015.11.016.

[16] Tian X, Jiang X, Welch C, Croley TR, Wong T-Y, Chen C, et al. Bactericidal effects of silver nanoparticles on Lactobacilli and the underlying mechanism. ACS Appl Mater Interfaces 2018;10(10):8443–50. doi: https://doi.org/10.1021/acsami.7b1727410.1021/acsami.7b17274.s001.

[17] El-Batal AI, Mosallam FM, El-Sayyad GS. Synthesis of metallic silver nanoparticles by fluconazole drug and gamma rays to inhibit the growth of multidrug-resistant microbes. J Clust Sci 2018;29(6):1003–15. doi: https://doi.org/10.1007/s10876-018-1411-5.

[18] Vazquez-Munoz R, Lopez FD, Lopez-Ribot JL. Silver nanoantibiotics display strong antifungal activity against the emergent multidrug-resistant yeast Candida auris under both planktonic and biofilm growing conditions. Front Microbiol 2020;11. doi: https://doi.org/10.3389/fmicb.2020.01673.

[19] Chen Y, Kistler HC, Ma Z. Fusarium graminearum trichothecene mycotoxins: Biosynthesis, regulation, and management. Annu Rev Phytopathol 2019;57 (1):15–39. doi: https://doi.org/10.1146/annurev-phyto-082718-100318.

[20] Liu Z, Jian Y, Chen Y, Kistler HC, He P, Ma Z, et al. A phosphorylated transcription factor regulates sterol biosynthesis in Fusarium graminearum. Nat Commun 2019;10:1–17. doi: https://doi.org/10.1038/s41467-019-09145-6.

[21] Duan Y, Lu F, Zhou Z, Zhao H, Zhang J, Mao Y, et al. Quinone outside inhibitors affect don biosynthesis, mitochondrial structure and toxisome formation in Fusarium graminearum. J Hazard Mater 2020;398:122908. doi: https://doi.org/10.1016/j.jhazmat.2020.122908.

[22] Zhang Y-J, Yu J-J, Zhang Y-N, Zhang X, Cheng C-J, Wang J-X, et al. Effect of carbendazim resistance on trichothecene production and aggressiveness of Fusarium graminearum. Mol Plant Microbe Interact 2009;22(9):1143–50. doi: https://doi.org/10.1094/MPMI-22-9-1143.

[23] Ibrahim E, Zhang M, Zhang J, Hossain A, Qiu W, Chen Y, et al. Green-synthesization of silver nanoparticles using endophytic bacteria isolated from garlic and its antifungal activity against wheat fusarium head blight pathogen Fusarium graminearum. Nanomaterials (Basel) 2020;10(2):219. doi: https://doi.org/10.3390/nano10020219.

[24] Lakshmeesha TR, Kalagatur NK, Mudili V, Mohan CD, Rangappa S, Prasad BD, et al. Biofabrication of zinc oxide nanoparticles with syzygium aromaticum flower buds extract and finding its novel application in controlling the growth and mycotoxins of Fusarium graminearum. Front Microbiol 2019;10. doi: https://doi.org/10.3389/fmicb.2019.01244.

[25] Yun Y, Liu Z, Yin Y, Jiang J, Chen Y, Xu J-R, et al. Functional analysis of the Fusarium graminearum phosphatome. New Phytol 2015;207(1):119–34. doi: https://doi.org/10.1111/nph.13374.

[26] Yu J-H, Hamari Z, Han K-H, Seo J-A, Reyes-Domínguez Y, Scazzocchio C. Double-joint PCR: A PCR-based molecular tool for gene manipulations in filamentous fungi. Fungal Genet Biol 2004;41(11):973–81. doi: https://doi.org/10.1016/j.fgb.2004.08.001.

[27] Yun Y, Liu Z, Zhang J, Shim W-B, Chen Y, Ma Z. The MAPKK FgMkk1 of Fusarium graminearum regulates vegetative differentiation, multiple stress response, and virulence via the cell wall integrity and high-osmolarity glycerol signaling pathways. Environ Microbiol 2014;16(7):2023–37. doi: https://doi.org/10.1111/1462-2920.12334.

[28] Wang J, Wang H, Zhang C, Wu T, Ma Z, Chen Y. Phospholipid homeostasis plays an important role in fungal development, fungicide resistance and virulence in Fusarium graminearum. Phytopathol Res 2019;1(1). doi: https://doi.org/10.1186/s42483-019-0023-9.

[29] Livak KJ, Schmittgen TD. Analysis of relative gene expression data using real-time quantitative PCR and the 2(-Delta Delta C(T)) method. Methods 2001;25:402–8. doi: https://doi.org/10.1006/meth.2001.1262.

[30] Shin J-H, Han J-H, Lee JK, Kim KS. Characterization of the maize stalk rot pathogens Fusarium subglutinans and F. Temperatum and the effect of fungicides on their mycelial growth and colony formation. Plant Pathol J 2014;30(4):397–406. doi: https://doi.org/10.5423/PPJ.OA.08.2014.0078.

[31] Kovács D, Szőke K, Igaz N, Spengler G, Molnár J, Tóth T, et al. Silver nanoparticles modulate ABC transporter activity and enhance chemotherapy in multidrug resistant cancer. Nanomedicine 2016;12(3):601–10. doi: https://doi.org/10.1016/j.nano.2015.10.015.

[32] Feng Y-X, Wang Y, Geng Z-F, Zhang Di, Almaz B, Du S-S. Contact toxicity and repellent efficacy of Valerianaceae spp. to three stored-product insects and synergistic interactions between two major compounds camphene and bornyl acetate. Ecotoxicol Environ Saf 2020;190:110106. doi: https://doi.org/10.1016/j.ecoenv.2019.110106.

[33] Gautam N, Salaria N, Thakur K, Kukreja S, Yadav N, Yadav R, et al. Green silver nanoparticles for phytopathogen control. Proc Natl Acad Sci, India, Sect B Biol Sci 2020;90(2):439–46. doi: https://doi.org/10.1007/s40011-019-01115-8.

[34] Ene IV, Walker LA, Schiavone M, Lee KK, Martin-Yken H, Dague E, et al. Cell wall remodeling enzymes modulate fungal cell wall elasticity and osmotic stress resistance. mBio 2015;6(4). doi: https://doi.org/10.1128/mBio.00986-15.

[35] Fischer-Parton S, Parton RM, Hickey PC, Dijksterhuis J, Atkinson HA, Read ND. Confocal microscopy of FM4-64 as a tool for analysing endocytosis and vesicle trafficking in living fungal hyphae. J Microsc 2000;198(3):246–59. doi: https://doi.org/10.1046/j.1365-2818.2000.00708.x.

[36] Takeshita N, Diallinas G, Fischer R. The role of flotillin FloA and stomatin StoA in the maintenance of apical sterol-rich membrane domains and polarity in the filamentous fungus Aspergillus nidulans. Mol Microbiol 2012;83:1136–52. doi: https://doi.org/10.1111/j.1365-2958.2012.07996.x.

[37] Stubbs RT, Yadav M, Krishnamurthy R, Springsteen G. A plausible metal-free ancestral analogue of the Krebs cycle composed entirely of α-ketoacids. Nat Chem 2020;12(11):1016–22. doi: https://doi.org/10.1038/s41557-020-00560-7.

[38] Liu C, Talbot NJ, Chen X-L. Protein glycosylation during infection by plant pathogenic fungi. New Phytol 2021;230(4):1329–35. doi: https://doi.org/10.1111/nph.v230.410.1111/nph.17207.

[39] Yin Y, Wang Z, Cheng D, Chen X, Chen Y, Ma Z. The ATP-binding protein FgArb1 is essential for penetration, infectious and normal growth of Fusarium graminearum. New Phytol 2018;219(4):1447–66. doi: https://doi.org/10.1111/nph.2018.219.issue-410.1111/nph.15261.

[40] El-Awady R, Saleh E, Hashim A, Soliman N, Dallah A, Elrasheed A, et al. The role of eukaryotic and prokaryotic ABC transporter family in failure of chemotherapy. Front Pharmacol 2016;7:535. doi: https://doi.org/10.3389/fphar.2016.00535.

[41] Gonçalves BM F, Cardoso DS P, Ferreira M-JU. Overcoming multidrug resistance: flavonoid and terpenoid nitrogen-containing derivatives as ABC transporter modulators. Molecules 2020;25(15):3364. doi: https://doi.org/10.3390/molecules25153364.

[42] Yun Y, Guo P, Zhang J, You H, Guo P, Deng H, et al. Flippases play specific but distinct roles in the development, pathogenicity, and secondary metabolism of Fusarium graminearum. Mol Plant Pathol 2020;21(10):1307–21. doi: https://doi.org/10.1111/mpp.12985.

[43] Audenaert K, Vanheule A, Höfte M, Haesaert G. Deoxynivalenol: A major player in the multifaceted response of Fusarium to its environment. Toxins (Basel) 2013;6:1–19. doi: https://doi.org/10.3390/toxins6010001.

[44] Ahmed B, Hashmi A, Khan MS, Musarrat J. ROS mediated destruction of cell membrane, growth and biofilms of human bacterial pathogens by stable metallic AgNPs functionalized from bell pepper extract and quercetin. Adv Powder Technol 2018;29(7):1601–16. doi: https://doi.org/10.1016/j.apt.2018.03.025.

[45] Jiang C, Zhang S, Zhang Q, Tao Y, Wang C, Xu J-R. FgSkn7 and FgAtf1 have overlapping functions in ascosporogenesis, pathogenesis and stress responses in Fusarium graminearum. Environ Microbiol 2015;17(4):1245–60. doi: https://doi.org/10.1111/1462-2920.12561.

[46] Cavassin ED, de Figueiredo LF, Otoch JP, Seckler MM, de Oliveira RA, Franco FF, et al. Comparison of methods to detect the in vitro activity of silver nanoparticles (AgNPs) against multidrug resistant bacteria. J Nanobiotechnol 2015;13:64. doi: https://doi.org/10.1186/s12951-015-0120-6.

[47] Velmurugan P, Anbalagan K, Manosathyadevan M, Lee K-J, Cho M, Lee S-M, et al. Green synthesis of silver and gold nanoparticles using Zingiber officinale root extract and antibacterial activity of silver nanoparticles against food pathogens. Bioprocess Biosyst Eng 2014;37(10):1935–43. doi: https://doi.org/10.1007/s00449-014-1169-6.

[48] Mishra M, Kumar S, Majhi RK, Goswami L, Goswami C, Mohapatra H. Antibacterial efficacy of polysaccharide capped silver nanoparticles is not compromised by AcrAB-TolC efflux pump. Front Microbiol 2018;9:823. doi: https://doi.org/10.3389/fmicb.2018.00823.

[49] Radhakrishnan VS, Reddy Mudiam MK, Kumar M, Dwivedi SP, Singh SP, Prasad T. Silver nanoparticles induced alterations in multiple cellular targets, which are critical for drug susceptibilities and pathogenicity in fungal pathogen (Candida Albicans). Int J Nanomedicine 2018;13:2647–63. doi: https://doi.org/10.2147/IJN.S150648.

[50] Some S, Sarkar B, Biswas K, Jana TK, Bhattacharjya D, Dam P, et al. Bio-molecule functionalized rapid one-pot green synthesis of silver nanoparticles and their efficacy toward the multidrug resistant (MDR) gut bacteria of silkworms (Bombyx Mori). RSC Adv 2020;10(38):22742–57. doi: https://doi.org/10.1039/D0RA03451G.

[51] Chand DT, Anu K, Majumdar RS, Vinod Y. Mechanistic basis of antimicrobial actions of silver nanoparticles. Front Microbiol 2016;7:1831. doi: https://doi.org/10.3389/fmicb.2016.01831.

[52] Durán N, Marcato PD, De Souza GIH, Alves OL, Esposito E. Antibacterial effect of silver nanoparticles produced by fungal process on textile fabrics and their effluent treatment. J Biomed Nanotechnol 2007;3(2):203–8. doi: https://doi.org/10.1166/jbn.2007.022.

[53] Ibrahim E, Luo J, Ahmed T, Wu W, Yan C, Li B. Biosynthesis of silver nanoparticles using onion endophytic bacterium and its antifungal activity against rice pathogen Magnaporthe oryzae. J Fungi (Basel) 2020;6:294. doi: https://doi.org/10.3390/jof6040294.

[54] Yang H, Liu C, Yang D, Zhang H, Xi Z. Comparative study of cytotoxicity, oxidative stress and genotoxicity induced by four typical nanomaterials: The role of particle size, shape and composition. J Appl Toxicol 2009;29(1):69–78. doi: https://doi.org/10.1002/jat.v29:110.1002/jat.1385.

[55] Jo Y-K, Kim BH, Jung G. Antifungal activity of silver ions and nanoparticles on phytopathogenic fungi. Plant Dis 2009;93(10):1037–43. doi: https://doi.org/10.1094/PDIS-93-10-1037.

[56] Bocate KP, Reis GF, de Souza PC, Oliveira Junior AG, Durán N, Nakazato G, et al. Antifungal activity of silver nanoparticles and simvastatin against toxigenic species of Aspergillus. Int J Food Microbiol 2019;291:79–86. doi: https://doi.org/10.1016/j.ijfoodmicro.2018.11.012.

[57] Mahdizadeh V, Safaie N, Khelghatibana F. Evaluation of antifungal activity of silver nanoparticles against some phytopathogenic fungi and *Trichoderma harzianum* URL. J Crop Prot 2015;4:291–300. http://jcp.modares.ac.ir/article-3-12407-en.html.

[58] Fernández JG, Fernández-Baldo MA, Berni E, Camí G, Durán N, Raba J, et al. Production of silver nanoparticles using yeasts and evaluation of their antifungal activity against phytopathogenic fungi. Process Biochem 2016;51 (9):1306–13. doi: https://doi.org/10.1016/j.procbio.2016.05.021.

[59] Shen T, Wang Q, Li C, Zhou B, Li Y, Liu Y. Transcriptome sequencing analysis reveals silver nanoparticles antifungal molecular mechanism of the soil fungi *Fusarium solani* species complex. J Hazard Mater 2020;388:122063. doi: https://doi.org/10.1016/j.jhazmat.2020.122063.

[60] Khan AM, Korzeniowska B, Gorshkov V, Tahir M, Schrøder H, Skytte L, et al. Silver nanoparticle-induced expression of proteins related to oxidative stress and neurodegeneration in an in vitro human blood-brain barrier model. Nanotoxicology 2019;13(2):221–39. doi: https://doi.org/10.1080/17435390.2018.1540728.

[61] Zuberek M, Stępkowski TM, Kruszewski M, Grzelak A. Exposure of human neurons to silver nanoparticles induces similar pattern of ABC transporters gene expression as differentiation: Study on proliferating and post-mitotic luhmes cells. Mech Ageing Dev 2018;171:7–14. doi: https://doi.org/10.1016/j.mad.2018.02.004.

[62] Perlin DS, Rautemaa-Richardson R, Alastruey-Izquierdo A. The global problem of antifungal resistance: Prevalence, mechanisms, and management. Lancet Infect Dis 2017;17(12):e383–92. doi: https://doi.org/10.1016/S1473-3099(17)30316-X.

[63] Bugde P, Biswas R, Merien F, Lu J, Liu D-X, Chen M, et al. The therapeutic potential of targeting ABC transporters to combat multi-drug resistance. Expert Opin Ther Tar 2017;21(5):511–30. doi: https://doi.org/10.1080/14728222.2017.1310841.

[64] Whaley SG, Zhang Q, Caudle KE, Rogers PD. Relative contribution of the ABC transporters Cdr1, Pdh1, and Snq2 to azole resistance in *Candida glabrata*. Antimicrob Agents Chemother 2018;62:e01070–e1118. doi: https://doi.org/10.1128/AAC.01070-18.

[65] Perlin MH, Andrews J, Toh SS. Essential letters in the fungal alphabet: ABC and MFS transporters and their roles in survival and pathogenicity. Adv Genet 2014;85:201–53. doi: https://doi.org/10.1016/B978-0-12-800271-1.00004-4.

[66] Klein C, Kuchler K, Valachovic M. ABC proteins in yeast and fungal pathogens. Essays Biochem 2011; 50: 101-119. doi: 10.1042/bse0500101.

[67] Dakal TC, Kumar A, Majumdar RS, Yadav V. Mechanistic basis of antimicrobial actions of silver nanoparticles. Front Microbiol 2016;7:1831. doi: https://doi.org/10.3389/fmicb.2016.01831.

[68] Gajbhiye M, Kesharwani J, Ingle A, Gade A, Rai M. Fungus-mediated synthesis of silver nanoparticles and their activity against pathogenic fungi in combination with fluconazole. Nanomed-Nanotechnol 2009;5(4):382–6. doi: https://doi.org/10.1016/j.nano.2009.06.005.

[69] Duan Y, Li T, Xiao X, Wu J, Li S, Wang J, et al. Pharmacological characteristics of the novel fungicide pyrisoxazole against *Sclerotinia sclerotiorum*. Pestic Biochem Physiol 2018;149:61–6. doi: https://doi.org/10.1016/j.pestbp.2018.05.010.

[70] Zhang C, Chen Y, Yin Y, Ji H-H, Shim W-B, Hou Y, et al. A small molecule species specifically inhibits *Fusarium* myosin I. Environ Microbiol 2015;17 (8):2735–46. doi: https://doi.org/10.1111/1462-2920.12711.

[71] Kovač T, Šarkanj B, Borišev I, Djordjevic A, Jović D, Lončarić A, et al. Fullerol C$_{60}$(OH)$_{24}$ nanoparticles affect secondary metabolite profile of important foodborne mycotoxigenic fungi in vitro. Toxins (Basel). 2020;12(4):213. doi: https://doi.org/10.3390/toxins12040213.

[72] Kovač T, Borišev I, Crevar B, Čačić Kenjerić F, Kovač M, Strelec I, et al. Fullerol C$_{60}$(OH)$_{24}$ nanoparticles modulate aflatoxin B1 biosynthesis in *Aspergillus flavus*. Sci Rep 2018;8(1). doi: https://doi.org/10.1038/s41598-018-31305-9.

[73] Das B, Khan MI, Jayabalan R, Behera SK, Yun S-I, Tripathy SK, et al. Understanding the antifungal mechanism of Ag@ZnO core-shell nanocomposites against *Candida krusei*. Sci Rep 2016;6(1). doi: https://doi.org/10.1038/srep36403.

[74] Audenaert K, Callewaert E, Höfte M, De Saeger S, Haesaert G. Hydrogen peroxide induced by the fungicide prothioconazole triggers deoxynivalenol (DON) production by *Fusarium graminearum*. BMC Microbiol 2010;10(1):112. doi: https://doi.org/10.1186/1471-2180-10-112.